




Article

Characteristic Aspects of Uranium(VI) Adsorption Utilizing Nano-Silica/Chitosan from Wastewater Solution

Ahmed K. Sakr ^{1,*}, Mostafa M. Abdel Aal ², Khaled A. Abd El-Rahem ³, Eman M. Allam ², Samia M. Abdel Dayem ², Emad A. Elshehy ², Mohamed Y. Hanfi ^{2,4}, Mohammed S. Alqahtani ^{5,6} and Mohamed F. Cheira ^{1,*}

¹ Department of Civil and Environmental Engineering, Wayne State University, 5050 Anthony Wayne Drive, Detroit, MI 48202, USA

² Nuclear Materials Authority, El Maadi, Cairo 11381, Egypt

³ Department of Chemistry, Faculty of Science, Al-Azhar University, Cairo 11651, Egypt

⁴ Institute of Physics and Technology, Ural Federal University, St. Mira, 19, 620002 Yekaterinburg, Russia

⁵ Department of Radiological Sciences, College of Applied Medical Sciences, King Khalid University, Abha 61421, Saudi Arabia

⁶ BioImaging Unit, Space Research Centre, University of Leicester, Michael Atiyah Building, Leicester LE1 7RH, UK

* Correspondence: ahmed.sakr@wayne.edu (A.K.S.); mf.farid2008@yahoo.com (M.F.C.)

Abstract: A new nano-silica/chitosan (SiO₂/CS) sorbent was created using a wet process to eliminate uranium(VI) from its solution. Measurements using BET, XRD, EDX, SEM, and FTIR were utilized to analyze the production of SiO₂/CS. The adsorption progressions were carried out by pH, SiO₂/CS dose, temperature, sorbing time, and U(VI) concentration measurements. The optimal condition for U(VI) sorption (165 mg/g) was found to be pH 3.5, 60 mg SiO₂/CS, for 50 min of sorbing time, and 200 mg/L U(VI). Both the second-order sorption kinetics and Langmuir adsorption model were observed to be obeyed by the ability of SiO₂/CS to eradicate U(VI). Thermodynamically, the sorption strategy was a spontaneous reaction and exothermic. According to the findings, SiO₂/CS had the potential to serve as an effectual sorbent for U(VI) displacement.

Keywords: chitosan; silicon dioxide; sorption; uranium; kinetics



Citation: Sakr, A.K.; Abdel Aal, M.M.; Abd El-Rahem, K.A.; Allam, E.M.; Abdel Dayem, S.M.; Elshehy, E.A.; Hanfi, M.Y.; Alqahtani, M.S.; Cheira, M.F. Characteristic Aspects of Uranium(VI) Adsorption Utilizing Nano-Silica/Chitosan from Wastewater Solution. *Nanomaterials* **2022**, *12*, 3866. <https://doi.org/10.3390/nano12213866>

Academic Editor: Ha-Jin Lee

Received: 10 October 2022

Accepted: 26 October 2022

Published: 2 November 2022

Publisher's Note: MDPI stays neutral with regard to jurisdictional claims in published maps and institutional affiliations.



Copyright: © 2022 by the authors. Licensee MDPI, Basel, Switzerland. This article is an open access article distributed under the terms and conditions of the Creative Commons Attribution (CC BY) license (<https://creativecommons.org/licenses/by/4.0/>).

1. Introduction

Nuclear power plants are a sustainable energy source and can produce more energy from uranium than any fossil fuel, including coal and petroleum oil. Furthermore, the increased costs of other renewable energy sources, such as wind, solar, and hydraulic, mean that nuclear energy is a better long-term investment. Their abundant energy resources are being depleted at an alarming rate due to ever-increasing global demand. Wastewater contains heavy metals alongside long-lived radionuclides, which are dangerous pollutants whose migration with groundwater is greatly influenced by adsorption on geological materials [1,2]. The removal of radioactive and toxic metals from wastewater is a major environmental concern [3,4]. Scientists are interested in developing several techniques for the treatment of wastewater [5–7]. Generally, wastewater comes from nuclear fuel production and laboratories that handle radioactive substances [8]. Uranium precipitation and removal from its leaner sources is now the focus of research and development on methods and composites that are more effective in the adsorption process [9–12].

Higher loading capacities can be achieved using adsorbents that allow fast reaction rates. Polymers and fibrous materials that are hydrophilic are excellent adsorbents because of their kinetics [13,14]. It is possible to classify sorbents based on their chemical composition into organic (natural polymers and synthetic polymers), inorganic (silica gel and other oxide species), and natural sorbents, such as white sand and clay, fall under the broad category of sorbents.

Cations are expected to be adsorbed by silica, while the most alkaline oxides (such as MgO) adsorb the anions due to their basic properties. Hydroxyl groups are thought to play a role in the adsorption of ions onto oxide surfaces [15]. The cations are retained when these groups are negatively charged (deprotonated), whereas the anions are retained when they are positively charged (protonated). As a result, on amphoteric oxides (e.g., Al₂O₃, TiO₂, and ZrO₂), cations are extracted under primary conditions (a pH higher than the oxide isoelectric point, which was noted to be 6.1 of TiO₂) [16]. On the other hand, anions can only be absorbed in acidic environments (pH below the isoelectric point of the oxide). The use of magnetic Fe₃O₄ and SiO₂ composites for removing U(VI) from solutions was investigated [17]. Using the solid-phase extraction approach, the sodium dodecyl sulfate/alumina/Schiff's base was used to determine the UO₂²⁺ ions in the environment [18].

The surfaces of montmorillonite, silica (SiO₂), and alumina were utilized to extract U(VI) at pH 3.1–6.3. According to these findings, ion exchange occurs during uranyl ion adsorption on montmorillonite at low pH, and the inner-sphere uranyl liquid structure is unaltered. pH values close to neutral and competing cations can lead to an inner-sphere complexation with the surface. According to uranyl adsorption on these surfaces, an inner-sphere, bidentate complexation of uranyl with silica and alumina surfaces appears to occur by forming polynuclear surface complexes with near-neutral pH [19]. Uranium was removed from the water solution and a mixture of aluminum hydroxide, ferric hydroxide, and activated carbon. The uranium extraction from dilute aqueous solutions was investigated using mixed adsorbent at various temperatures and pH levels. In the pH range of 4.0 to 5.5, the adsorbability peaked and then declined as the temperature rose. The best eluting solution was ammonium carbonate [20,21].

Furthermore, amidoxime-modified ordered mesoporous silica was produced and it proved the high uptake of uranium from seawater (57 mg/g). Mostly, mesosilica seems to be an excellent choice for the recovery of uranium from an aqueous solution [22–24]. Magnetic chitosan microparticles were functionalized by grafting either amidoxime or hydrazinyl amine onto them. U(VI) and Zr(IV) were recovered from the fluid solutions by testing the sorption characteristics in a pH range of 4.0–5.0 [25], poly sulfonamide/nano-silica composite was utilized to adsorb thorium ions from the sulfate solution [26,27].

Additionally, the U(VI) adsorption behavior on amino/silica SBA-15 was also reported. Many parameters were studied to determine the adsorption properties of U(VI) in discontinuous settings. When the grafted materials were exposed to U(VI), adsorption reached equilibrium in about 30 min, with the most effective material's extreme U(VI) sorption capacity of 573 mg/g and an ideal pH of 6.0. It has also been discovered that the adsorbed U(VI) is concentrated in the mesopores, generating nanometer-sized U-hydroxy phases [28]. The separation and preconcentration of radioactive uranium using salicylaldehyde/mesoporous silica sorbents were also achieved [29]. In this work, the nano-silica/chitosan (SiO₂/CS) preparation was described and used to adsorb U(VI) from the definite aqueous phase. The ideal variables for uranium sorption from standard solutions and the wastewater solution are also established, comprising pH, contact time, U(VI) concentration, and temperature.

2. Experimentation

2.1. Chemicals and Instruments

Analytical-grade chemicals and reagents were employed throughout the operation, with no further purifying in the lab. Merck, Germany, donated the chitin, sulfuric acid, and tetraethyl-orthosilicate used in this experiment. Uranyl sulfate and N-phenyl anthranilic acid were purchased from the B.D.H. lab., England.

Uranium was found using a JENWAY UV/Vis. 6405 spectrophotometer with quartz cells of 1 cm in diameter and a detection wavelength of 655 nm. These changes in the mineralogical composition were investigated using X-ray diffraction (XRD) on Bruker company model D8 (which also included reflection spectroscopy (RF), high-resolution diffraction (HRD), in-plane grating incidence diffraction (IP-GID), residual stress, and

texture measurements). IR resolution Software was used to analyze the adsorbents and create samples for FTIR characterization (Shimadzu I.R. Prestige21). An environmental scanning electron microscope (SEM-EDX) (Philips XL 30, Eindhoven, The Netherlands) was used to identify precipitated uranium qualitatively. Additionally, in addition, a quick qualitative investigation of the mineral sample was carried out using this method. Low vacuum and 30 KV were the operating conditions. Model Nova Touch LX2, manufactured by Quantachrome Corporation, Boynton Beach, FL, USA, operated by Windows®Version 1.12, Microsoft, Redmond, WA, USA, has been used to study surface area and pore volume of samples by nitrogen sorption at 77 K.

2.2. Chitosan Synthesis

Chitin deacetylation [30–33] was performed to achieve CS by stirring 20 g of chitin in 100 milliliters of a solution containing 50% sodium hydroxide. The mixture was held at a shallow temperature of $-85\text{ }^{\circ}\text{C}$ for 28 hr after being ultra-frozen to that temperature. After that, the mixture's temperature was increased to $112\text{ }^{\circ}\text{C}$, and it was agitated for 8 h at a rate of 275 revolutions per minute. The chitosan was filtered, rinsed with deionized H_2O adjacent to pH 7.0, and then dried in a furnace at $65\text{ }^{\circ}\text{C}$ once it had been obtained.

2.3. Nanosilica Synthesis

Hydrothermal synthesis yielded mesoporous, spherical nano-silica [34,35]. The suspension of cetyltrimethylammonium bromide (CTAB) in deionized water, with the addition of 1 M NaOH (10 mg/mL) and an equal volume of water, was carried out at $80\text{ }^{\circ}\text{C}$. The acceptable solution was then supplemented with 11.7 mL of TEOS and vigorously agitated before being added. The white precipitate was obtained by filtering after two hr of continuous rousing at $80\text{ }^{\circ}\text{C}$, and it was washed away at least three times with ethanol before drying for 12 h at $60\text{ }^{\circ}\text{C}$. The surfactant was removed by calcining the powder for 4.5 h at $600\text{ }^{\circ}\text{C}$, and the resulting fine powder was then tested for nano-silica using a spectrophotometric method.

2.4. Silica/Chitosan Synthesis

The sol-gel method was used to synthesize silica/chitosan [36,37]. Two different solutions were made using a unique method. First, 2 mL of water and hydrochloric acid were added to 60 mL of ethanol in the first solution for 10 min, stirring at 250 rpm at $25\text{ }^{\circ}\text{C}$. A magnetic stirrer was used to slowly add a total of 93 mL of tetraethyl orthosilicate (TEOS) to ensure that the mixture was evenly dispersed. In a rounded bottom flask, 30.0 g of chitosan powder was liquified in 500 mL acetic acid (5.0%) as a second liquid solution. After the chitosan was utterly dissolved in the diluted acetic acid solution, the mixture was agitated for another two hr. The dropwise addition of the first TEOS solution to the second chitosan solution resulted in silica/chitosan. The reactant mixture was agitated for 36 hr at 200 rpm after the solution had been poured in completely. To crosslink the gel, it was allowed to sit for a week before being dried at $55\text{ }^{\circ}\text{C}$. An airtight bottle labeled "silica/chitosan" held the finished powder.

2.5. Uranium Adsorption

This study used the batch approach to adsorb uranium from standard and leaching liquor solutions. U(VI) adsorption was studied by performing a number of experiments in order to determine the optimal values for a number of important factors that influence the sorption process. These variables included pH, contact time, adsorbent dose, and temperature. The mean value of each experiment was used in all cases. Adsorbent dosages of 10 to 100 mg were mixed with 50 mL of uranium solution of various concentrations and shaken at 200 rpm utilizing mechanical shakers for a period of time ranging from 5 to 120 min at various temperatures by ranging the ambient temperature between 25 and $55\text{ }^{\circ}\text{C}$. NaOH and H_2SO_4 solutions adjusted the pH from 1.0 to 6.0. The concentration of metal ions absorbed was determined by comparing the equilibrium and initial concentrations.

Different tests were performed on uranium ions to examine their adsorption dynamics, equilibrium isotherms, and thermodynamics by ranging the ambient temperature between 25 and 55 °C.

In each experiment, the adsorption capacity q_e (mg/g) and adsorption efficiency (E%), as well as the distribution coefficient (K_d) of uranium ions on the produced adsorbents, were calculated using the equations below:

$$q_e = (C_0 - C_e) \times \frac{V}{m} \quad (1)$$

$$E(\%) = \left(\frac{C_0 - C_e}{C_0} \right) \times 100 \quad (2)$$

$$K_d = \left(\frac{C_0 - C_e}{C_e} \right) \times \frac{v}{m} \quad (3)$$

This equation provides an easy-to-understand representation for C_0 and C_e as a function of volume (liters, V or milliliters, v), concentration (mg/L), as well as dry adsorbent weight (g).

2.6. Uranium Desorption

Desorption was executed on the uranium-loaded SiO_2/CS gained from the formerly reported set of processes researched to learn more about desorption. This process utilized sulfuric, hydrochloric, nitric acids, sodium carbonate, and ammonium carbonate as eluants. The uranium(VI)-loaded adsorbent was shaken at room temperature with 50 mL of eluent at various concentrations ranging from 0.2 to 1.2 M unless it is stated otherwise. The solid/liquid phase ratio was studied by ranging from 1:10 to 1:70 S/L phase ratio, while the elution time was studied by ranging from 10 to 120 min. The uranium ions were then eluted into the acid solution by filtering the solution. The uranium content was measured by Agilent 7800 ICP-MS, Santa Clara, CA, USA. This study examined the factors that affect uranium desorption, such as the eluent concentration, contact time, and temperature. All of the experiments were triplicated, and the mean value was used.

3. Results and Discussion

The newly prepared nano-silica/chitosan (SiO_2/CS) was characterized and used as an adsorbent for the removal of U(VI) ions from the wastewater solution. Different parameters such as the pH effect, contact time, U(VI) concentration, and temperature have been investigated.

3.1. Characteristics

3.1.1. X-ray Diffraction Analysis

Figure 1 displays the XRD forms of nano-silica (SiO_2), chitosan (CS), and nano-silica/chitosan (SiO_2/CS). These broad SiO_2 characteristic peaks are matching to Bruker software COD 9014256 database values of $2\theta = 19, 22, 24, 24.8, 28, 29, 32, 34, 36, 39, \text{ and } 49^\circ$. Cristobalite was found to make up most of SiO_2 , according to the data gathered from the SiO_2 pattern. In the database of Bruker software COD 7114110, 7150157, and 8100678, chitosan (CS) revealed a major broad peak at $2\theta = 19^\circ$. Figure 1 shows the XRD results of SiO_2/CS and $\text{U}/\text{SiO}_2/\text{CS}$. The peak location and peak form were unaffected by the broad peaks of SiO_2 that overlapped with the XRD pattern of CS, which had a high-intensity peak at $2\theta = 19^\circ$. In these data, the surface electrostatic interaction between SiO_2 with CS, which has broad peaks at $2\theta = 9$ and 20° , besides two little two peaks, appeared at $2\theta = 29^\circ$ and 35° , along with the relevant database of the Bruker program COD 4124041 and 4025951. It was found that some new peaks appeared in the XRD pattern of $\text{U}/\text{SiO}_2/\text{CS}$ following absorption, according to the Bruker program COD 8103695, 9000080, and 9009686. As opposed to this, there was only a small shift in peak intensities, showing that the composite SiO_2/CS crystallinity was unaffected by U(VI) adsorption.

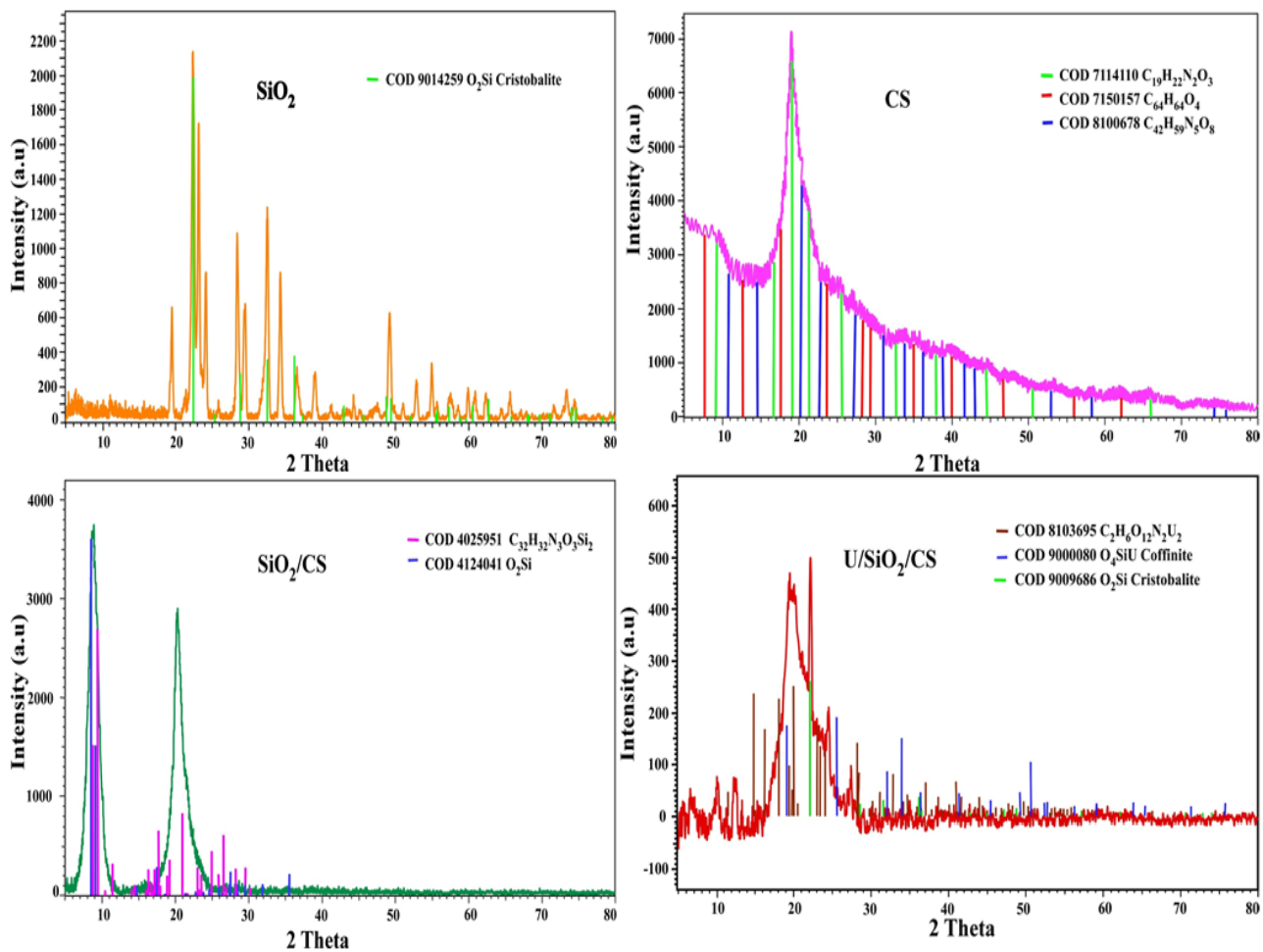


Figure 1. SiO_2 , CS, SiO_2/CS , and $\text{U}/\text{SiO}_2/\text{CS}$ XRD patterns.

3.1.2. EDX and SEM Images

Scanning electron microscopy is the most reliable and convenient tool for examining the physical structure of the resin beads modified in a solvent. In addition, as shown in Figure 2, SEM was used to investigate the surface and physical formations of SiO_2 and CS. SiO_2 SEM has revealed distinct shapes and compositions, including distinct roughness. The skeleton of SiO_2 was built from a variety of small, unrelated pieces with varying diameters. As shown in Figure 2, the surface CS has been smoothed by several holes. Due to the collection and impregnation of small SiO_2 molecules on the surface of CS, the SEM images show a smooth surface with several cavities. In addition, the composites photographed were made from aggregate particles with larger interstitial holes, as evidenced by the photographs after the SiO_2/CS was treated with U(VI) adsorption (SEM images revealed that the pores were occupied with U(VI), this composite had erratic surfaces that were agglomerated with U(VI).

Figure 2 illustrates the semi-quantitative analysis of SiO_2 , CS, SiO_2/CS , and $\text{U}/\text{SiO}_2/\text{CS}$. The spectra of SiO_2 showed just silicon and oxygen peaks; no other peaks could be seen. Additionally, the CS spectrum comprises N, C, and O peaks. C, O, Si, and N peaks were found in the EDX study of SiO_2/CS . Peaks in Si, N, C, and O can be found in the SiO_2/CS . There are separate peaks after uranium ion adsorption on SiO_2/CS . The uranium peaks confirmed uranium (VI) adsorption on SiO_2/CS .

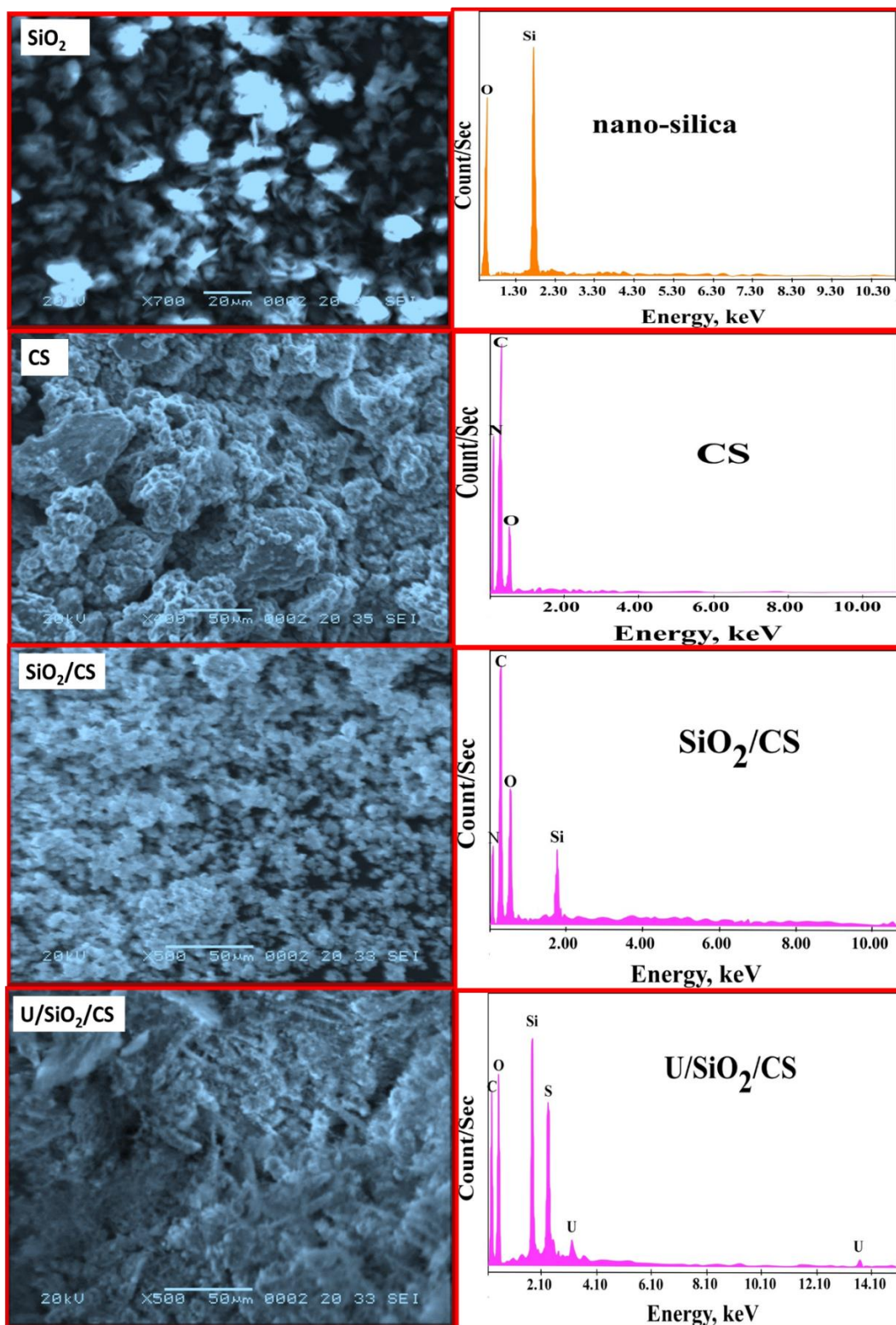


Figure 2. SEM and EDX photographs of SiO₂, CS, SiO₂/CS, and U/SiO₂/CS.

3.1.3. BET Surface Examination

To determine the surface area, BET was used. Information about the physical structure of the material can be achieved by studying its surface area, which determines how a solid will interact with its environment. Figure 3 presents the N₂ sorption-desorption

isotherm curvatures of the examined ingredients. After the CS was improved with SiO₂, the isotherms were altered.

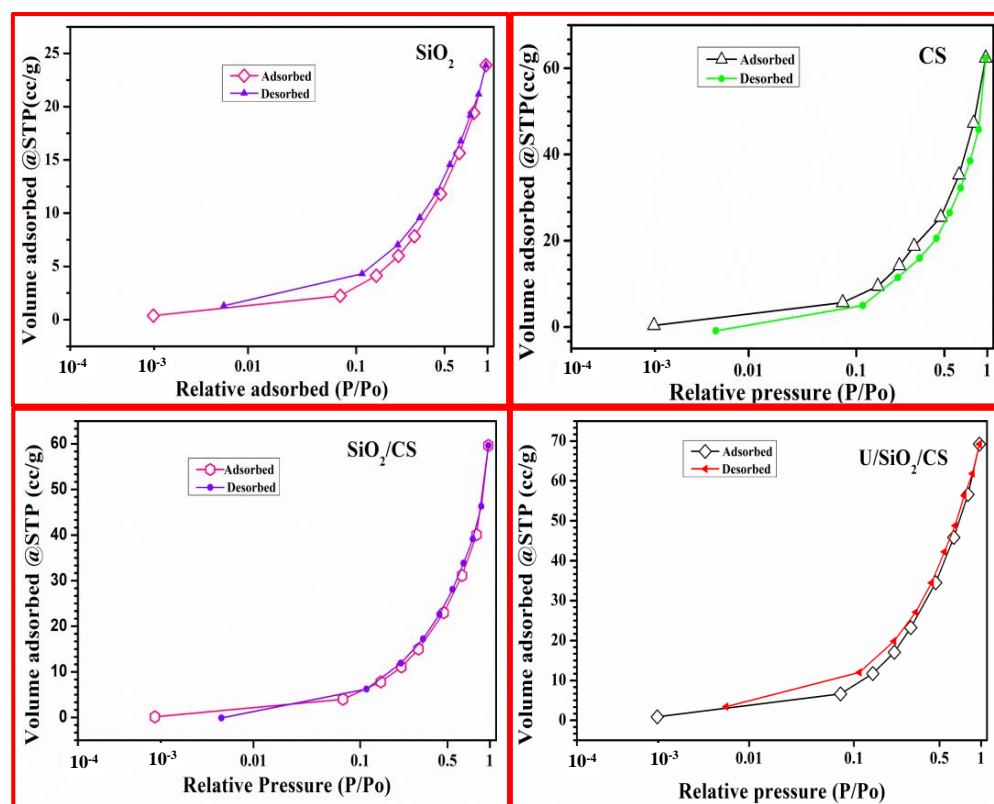


Figure 3. N₂ adsorption/desorption isotherm of SiO₂, CS, SiO₂/CS, and U/SiO₂/CS.

Table 1 revealed that the BET surface areas of SiO₂, CS, SiO₂/CS, and U/SiO₂/CS were 25.85, 19.77, 24.55, and 22.71 m²/g, respectively. The surface area (S_{BET}), pore volume, and pore size of SiO₂/CS were discernibly different from those of their constituents due to the addition of SiO₂ to the CS surface, the surface area has been enhanced, and the uranium ions were better able to adhere to it. This difference may be attributable to the fact that SiO₂ adorned CS pores. The adsorption of uranium ions adsorption reduced, to some extent, the surface area, pore size, and pore volume. SiO₂/CS is strongly adsorbable to U(VI) ions because of the number of active sites.

Table 1. Surface parameters of SiO₂, CS, SiO₂/CS, and U/SiO₂/CS.

Materials	S_{BET} , m ² /g	Pore Size, nm	Pore Volume, cc/g
SiO ₂	25.85 ± 0.21	2.87 ± 0.08	0.037 ± 0.006
CS	19.77 ± 0.32	2.65 ± 0.09	0.033 ± 0.005
SiO ₂ /CS	24.55 ± 0.43	2.75 ± 0.07	0.035 ± 0.007
U/SiO ₂ /CS	22.71 ± 0.26	2.59 ± 0.08	0.032 ± 0.008

3.1.4. FTIR Investigation

FTIR spectroscopy was also exploited to assess the nano-SiO₂, CS, SiO₂/CS, and U/SiO₂/CS, as seen in Figure 4. An extensive band at 3450 cm⁻¹ was attributed to SiOH stretching, while a distinctive band of H₂O on SiO₂ was observed at 1646 cm⁻¹ that was not completely displaced by drying [38]. At 1216 and 1088 cm⁻¹, the siloxane molecular group (Si–O–Si) was clearly visible [39]. Furthermore, the silanol group was recorded as having an attendance peak of 956 cm⁻¹ (SiOH). The vibrational motion of the Si–O–Si group was responsible for both the peak position at 795 cm⁻¹ and the observed peak at 466 cm⁻¹ [40].

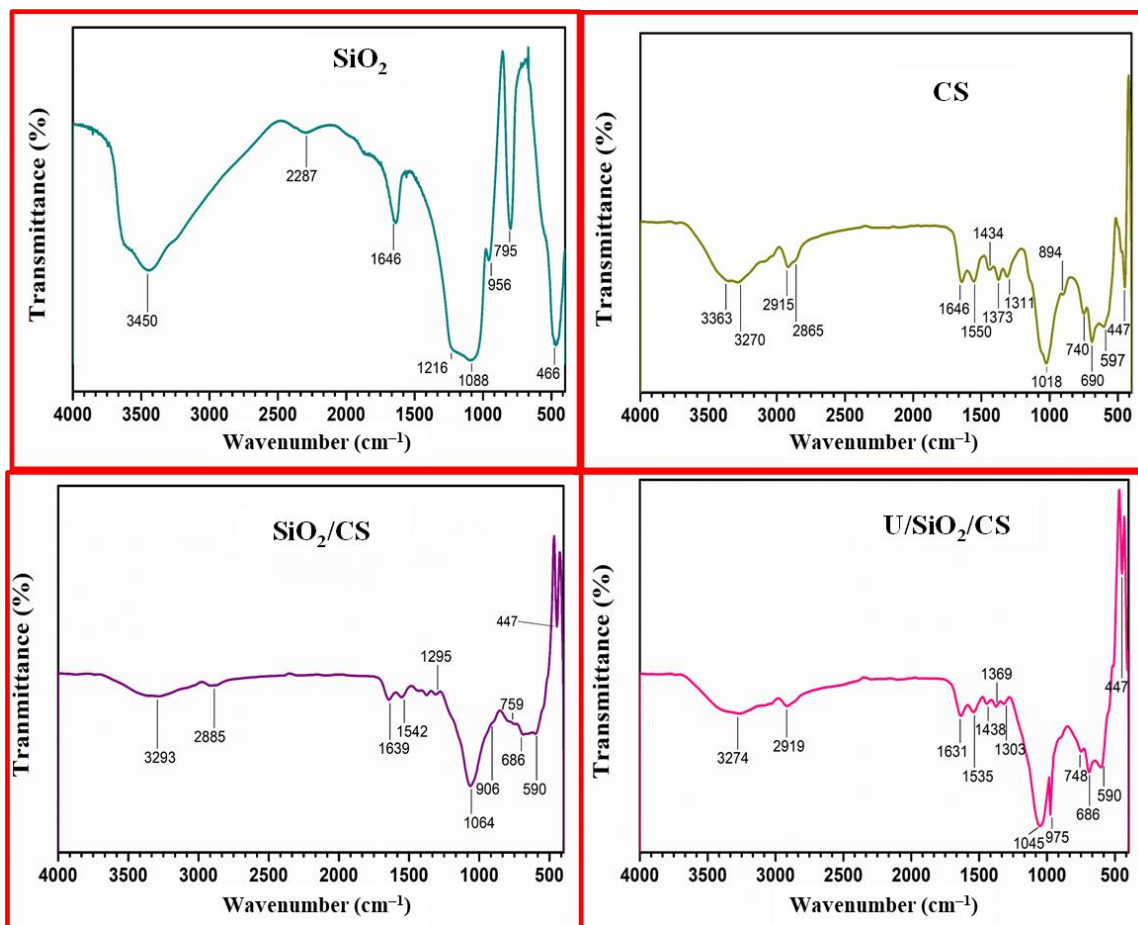


Figure 4. SiO_2 , CS, SiO_2/CS , and $\text{U}/\text{SiO}_2/\text{CS}$ FTIR spectra.

There was a noticeable FTIR peak around $3200\text{--}3550\text{ cm}^{-1}$ because of the overlap of OH and NH groups [41]. The peaks at 2915 cm^{-1} and 2865 cm^{-1} were assigned to $-\text{CH}_2$ groups. The distinctive peak at 1646 cm^{-1} is related to the NH_2 , and 1434 cm^{-1} corresponds to the deformation peak of NH [42]. The peaks at 1550 cm^{-1} and 1166 cm^{-1} , and 1018 cm^{-1} fit the stretching C–N, respectively [43]. The stretching vibrations of C–O and C–O–C are also responsible for the 1373 and 1311 cm^{-1} peaks. The characteristic absorption of the d-glucose unit was found in the absorption band at 894 cm^{-1} [44].

In contrast, the FTIR scale of SiO_2/CS demonstrated a broad peak (3292 cm^{-1}) belonging to the overlapping of OH of SiO_2 and NH of CS. Peaks at 1295 cm^{-1} and 1064 cm^{-1} pointed to the siloxane groups (Si–O–Si). Additionally, the predicted Si–OH peak at 906 cm^{-1} matched the Si–O–Si group, and the absorption peak at 759 cm^{-1} was found to be a match. The OH and NH stretching vibration bands of the investigated adsorbents were reduced and shifted to a redshift with $5\text{--}10\text{ cm}^{-1}$ after U(VI) adsorption, which may be due to the pickup of U(VI) to the surface adsorbents, as shown in the spectra of $\text{U}/\text{SiO}_2/\text{CS}$ after U(VI) adsorption. In addition, new peaks of (O=U=O) were discovered at 975 and 748 cm^{-1} [45]. Moreover, two weak peaks appeared of U–O near $= 490\text{ cm}^{-1}$ [46]. Thus, NH_2 , NH, and $-\text{OH}$, groups are reactants with uranyl cations in this reaction. Accordingly, it realized that the modified CS has the ability to adsorb U(VI) ions.

3.2. U(VI) Sorption

3.2.1. Influence of pH

The influence of pH on the U(VI) sorption efficacy from the standard solution is exhibited in Figure 5a. Numerous tests were carried out at pH levels ranging from 1.0 to 6.0, with mixed results. This was conducted in conjunction with maintaining the other

conditions constant, such as the 50 mL solution concentration, measuring 200 mg/L U(VI), and 30 min contact time at room temperature with a SiO₂/CS adsorbent dose (0.05 g). It has been found that by increasing the pH from 1.0 to 3.5, the adsorption efficiency of U(VI) ions has consistently increased from 13.0% to 62.5%. It is noteworthy that at high acidity, the functional group of SiO₂/CS is protonated and competes with uranium anions complexes for adsorption. The condensed uptake was facilitated by the active sites of SiO₂/CS. Conversely, the adsorption effectiveness was reduced by raising the pH to 6.0 due to the hydrolysis of cationic UO₂²⁺ and (UO₂)₂(OH)₂²⁺ species to UO₂(OH)⁺, (UO₂)₃(OH)₅⁺, (UO₂)₄(OH)₇⁺, and UO₂(OH)₂ species. Consequently, pH 3.5 is selected as an optimum pH value in the procedures of the subsequent experiments.

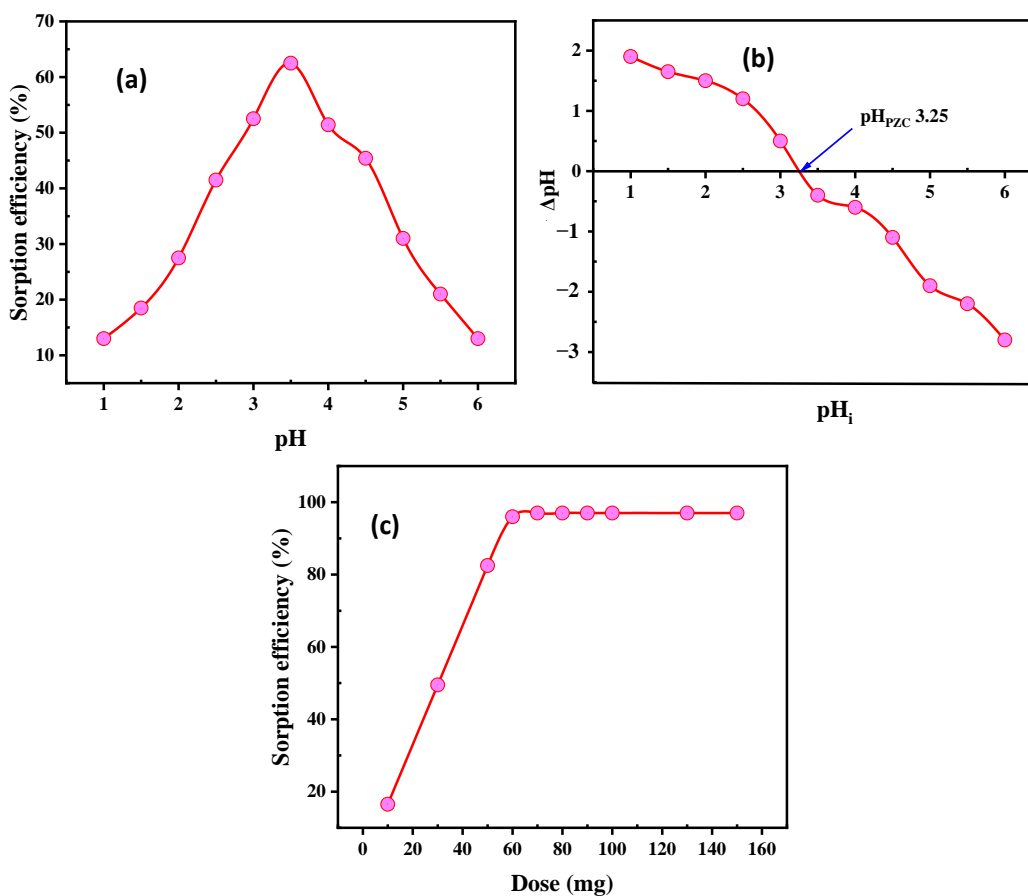


Figure 5. Influence of (a) pH, (b) pH_i and (c) SiO₂/CS dose on the U(VI) sorption exploiting SiO₂/CS.

The pH at which the net surface charge of the adsorbent is equal to zero is referred to as the pH at the point-of-zero-charge (pH_{PZC}). When electrostatic interactions are the major adsorption mechanism, the pH_{PZC} value becomes a crucial metric for interpreting the interactions that take place at the surfaces of materials, particularly for charged adsorbate species. When the pH of the solution is greater than pH_{PZC}, the surface of the adsorbent exhibits a negative surface charge due to the adsorption of OH⁻ ions or the deprotonation of hydrogen ions. Under conditions in which pH is lower than pH_{PZC}, the surface of the adsorbent exhibits a positive surface charge because of the adsorption of hydrogen ions from the solution [46,47]. It would be very beneficial to identify the point of zero charges (pH_{PZC}) of the SiO₂/CS to calculate the ideal pH for U(VI) sorption. This can be undertaken by determining the value of the pH_{PZC}. For the purpose of deriving the pH_{PZC} value, a plot of the pH change observed after equilibration (pH_f) and the initial (pH_i) against the initial pH value (pH_i) of the solutions was utilized. It was discovered that the pH_{PZC} of SiO₂/CS was roughly equivalent to 3.25 (Figure 5b). If the pH were less than pH_{PZC}, the SiO₂/CS would have a positive charge, but if the pH were greater than pH_{PZC}, the charge

would be negative. Therefore, it is understandable that U(VI) ions are substantially and thermodynamically more practicable to accumulate on the surface at pH values higher than the pH_{PZC} value. Despite this, the efficiency of uranium sorption continues to decline with increasing pH that is greater than pH 3.5. It is because of the progressive creation of the hydroxide precipitate of U(VI). Therefore, it would have a neutral charge at a pH of 3.25 (low charge density), which would demonstrate that the primary mechanism for binding metal ions and their enrichment is complexation with the OH and amino groups. Therefore, a pH of 3.5 is preferable for adsorption purposes.

3.2.2. Influence of SiO₂/CS Dose

The U(VI) adsorption efficiency was studied under constant conditions of pH 3.5 and 50 mL using a solution containing 200 mg/L U(VI) for 50 min of room temperature contact time in a series of experiments using adsorbent doses of SiO₂/CS ranging from 10 to 150 mg (Figure 5c). U(VI) adsorption efficiency improved with increasing SiO₂/CS dose. The adsorption efficiency increased gradually to 60 mg of SiO₂/CS, remaining constant after that point. As a result, the recommended dose of SiO₂/CS was 60 mg.

3.2.3. Contact Time

The effects of the contact time on SiO₂/CS U(VI) adsorption were investigated at 5 to 120 min. At room temperature and with SiO₂/CS doses of 60 mg/L and U(VI) ion concentrations of 200 mg/L, the other adsorption parameters were varied, but all were set to pH 3.5. To reach equilibrium at 50 min (as shown in Figure 6a), U(VI) adsorption improved with increasing contact time. As a result, the minimum time required for additional work was 50 min.

The adsorption processes and rate-controlling steps were studied using kinetic models to determine the mechanism and rate-controlling steps. For the kinetic adsorption mechanism of U(VI) adsorption on SiO₂/CS, first- and second-order kinetic models were used. The first-order model is given in the linear form, as in the resulting equation [48]:

$$\log(q_e - q_t) = \log q_e - \left(\frac{k_1}{2.303}\right)t \quad (4)$$

The first-order rate constants k_1 (min^{-1}) and q_e (mg/g U(VI) at equilibrium and time t (min), respectively, are q_e and q_t . The slope and intercept can be used to calculate k_1 and q_e using the $\log(q_e - q_t)$ vs. t relationship. The correlation coefficient R^2 and q_e values obtained in Figure 6b show that they do not fit a first-order kinetic model. According to the objective findings, the first-order reaction cannot be carried out using U(VI) adsorption on SiO₂/CS.

The second-order kinetic model, on the other hand, is implemented and built up in the following equation [49]:

$$\frac{t}{q_t} = \frac{1}{k_2 q_e^2} + \left(\frac{1}{q_e}\right)t \quad (5)$$

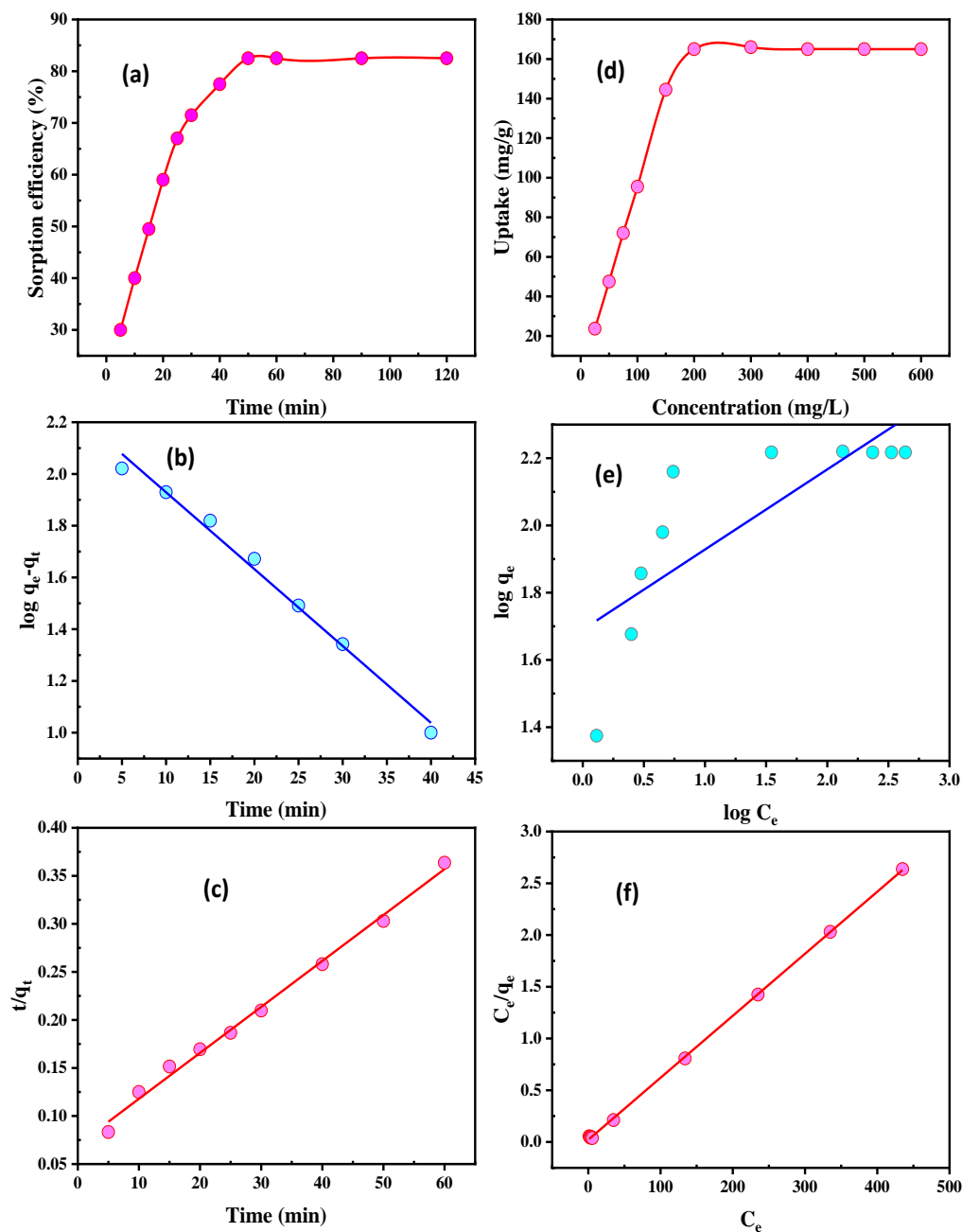


Figure 6. (a) Time influence, (b) first-order kinetic, (c) second-order kinetic, (d) U(VI) concentration influence, (e) Freundlich isotherm, and (f) Langmuir isotherm on U(VI) adsorption using SiO₂/CS.

Here, q_t (mg/g) is the amount of U(VI) adsorbed at time t (min), and q_e (mg/g) is the amount of U(VI) adsorbed at equilibrium. Chemical adsorption is the rate-dominant step, and this design can predict the kinetic uptake of adsorption. The t/q_t vs. t relationship was provided in straight lines when the second-order reaction was valid. The q_e and k_2 were calculated by intercepting and the slope. Figure 6c and Table 2 show a correlation coefficient (R^2) close to unity, and the calculated value of adsorbed amounts at equilibrium is closer to the practical capacity than the theoretical ones. According to these findings, U(VI) adsorption on SiO₂/CS was in good accordance with the second-order kinetic.

Table 2. For U(VI) adsorption Kinetic parameters of SiO₂/CS.

Pseudo-1st-Order			Pseudo-2nd-Order		
q _{e(cal)} (mg/g)	k ₁ (1/min)	R ²	q _{e(cal)} (mg/g)	k ₂ (g/mg.min)	R ²
106.19	0.068	0.942	181.82	5.69 × 10 ⁻⁴	0.995

3.2.4. U(VI) Concentration Influence

This is a crucial parameter of the adsorption technique, and it can affect the adsorption performance of uranium ions. Several batch tests were conducted using 60 mg of SiO₂/CS to determine the effect of U(VI) concentration on adsorption efficiency. The standard solution of uranium ions in the range of 25 to 600 mg/L at a pH value of 3.5 was shaken for 50 min at room temperature to conduct these tests. According to Figure 6d, as the uranium ion concentration rose, the adsorption efficiency peaked at 200 mg/L. At 200 mg/L, SiO₂/CS had the highest adsorption efficiency, at 82.5%. Additionally, the experimental loading capacity of SiO₂/CS was 165.0 mg/g. Uranium ions completely blocked SiO₂/CS because the solution's uranium mobility was the highest.

Adsorption isotherms are effectual systems for the adsorption reaction by ion transfer to the adsorbents [50]. The adsorption isotherms were studied to identify relevant data for adsorption when the adsorbed ions were spread within the solid and aqueous phases when the adsorption process reached equilibrium. The adsorption technique was studied using the models Freundlich and Langmuir. The Freundlich isotherm describes the adsorption of U(VI) on the adsorbent surface [51]. It is commonly utilized to study surface energies and heterogeneity [52,53]. To identify the Freundlich isotherm, the following equation was used:

$$\log q_e = \log K_f + \frac{1}{n} \log C_e \quad (6)$$

The amount of U(VI) adsorbed at equilibrium (q_e) is the amount of U(VI) adsorbed at equilibrium (mg/g), and U(VI) concentration in solution (C_e) is the constant related to maximum adsorption capacity (K_f). The regression lines for n and K_f were drawn from the log q_e vs. log C_e curve. The R² value was calculated using data from Table 3 and Figure 6e and was found to be 0.641. Consequently, the results showed that the Freundlich isotherm was not applicable in this case.

Table 3. U(VI) adsorption isotherm parameters of SiO₂/CS.

Freundlich			Langmuir		
K _f (mg/g)	n (mg.min/g)	R ²	q _{max}	b (L/mg)	R ²
48.99 ± 2.13	4.196 ± 0.93	0.641	166.66 ± 3.77	0.290 ± 0.04	0.9998

Saturated monolayer adsorption on adsorbent surfaces under constant energy conditions is the basis of the Langmuir isotherm model's ion uptake on a homogenous surface. On the surface, there is no ion association. The following equation quantifies it as follows:

$$\frac{C_e}{q_e} = \frac{1}{q_{\max} b} + \left(\frac{1}{q_{\max}} \right) C_e \quad (7)$$

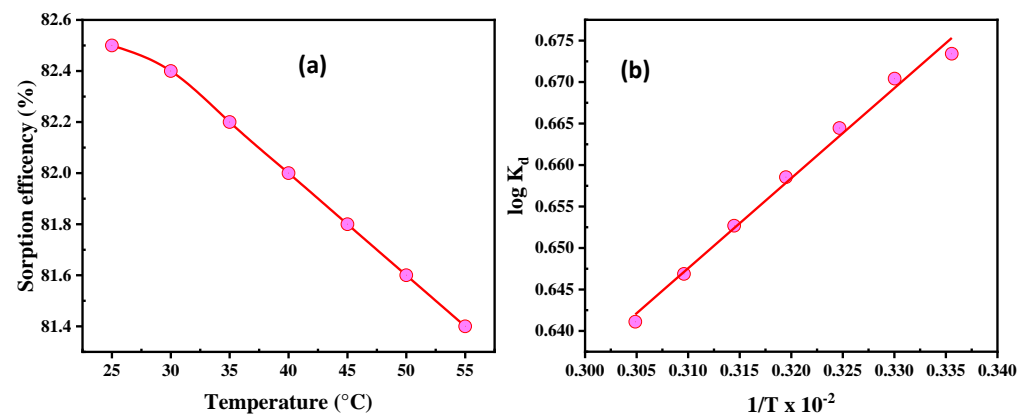
U(VI) adsorbed/unit mass of adsorbent q_e (mg/g) equilibrium, q_{max} (mg/g) maximum, and b is a constant linked to the affinity of the binding sites and adsorption energy (mg/L). There was a close match between the uptake capacity (166.66 mg/g) and experimental uptake capacity (165.0 mg/g), and the R² was closer to unity. The Langmuir isotherm was clearly observed in U(VI) adsorption. In this work, the uptake capacity is regarded as having achieved a good level of attainment because it has been compared to the data on the uranium uptake provided by other researchers (Table 4).

Table 4. Comparison of U(VI) uptake capacity of SiO₂/CS among other adsorbents.

Sorbent	Uptake (mg/g)	References
Free silica gel	21.40	[19]
Nanoporous silica	29.40	[54]
SiO ₂ /graphene oxide	145.00	[34]
Triamine modified silica (TAMS)	90.30	[55]
Pentamine modified silica (PAMS)	112.00	[55]
Chitosan	68.0	[56]
ZrO ₂ /Chitosan	175.00	[57]
Deacetylated chitosan	17.44	[58]
Amidoxime/chitosan/bentonite	49.09	[59]
Chitosan/attapulgit	53.5	[60]
SiO ₂ /CS	165.00	This work

3.2.5. Temperature and Thermodynamics

Temperatures ranging from 25 to 55 °C were used to examine the effect of temperature on the adsorption of U(VI). As a result, 50 mL of water was used for the experiments, which were run for 50 min with constant concentrations of 200 mg/L U(VI), pH 3.5, and a SiO₂/CS dose of 0.05 g (Figure 7a). By raising the temperature to 55 °C, the adsorption rate drops from 82.5 to 81.4%. However, the breakdown of van der Waals bonds leads to a decrease in the number of active sites. As a result, the ideal sorption temperature is found in the ambient air.

**Figure 7.** (a) Temperature influence, and (b) thermodynamic relation for U(VI) adsorption on SiO₂/CS.

The changes in Gibbs free energy (ΔG°), energy enthalpy (ΔH°), and dispersion were measured using adsorption trails at various temperatures for each of the three thermodynamic quantities. The following were determined to be the thermodynamic conditions for U(VI) adsorption [61,62]:

$$\log K_d = \frac{\Delta S^\circ}{2.303R} - \frac{\Delta H^\circ}{2.303RT} \quad (8)$$

$$\Delta G^\circ = \Delta H^\circ - T\Delta S^\circ \quad (9)$$

K_d and R are the adsorption equilibrium constant (L/g) and universal gas constant (8.314 J/mol.K), respectively. T stands for the absolute value of a given quantity (K). The negative ΔG° values in Figure 7b and Table 5 indicate that U(VI) adsorption is spontaneous. Because the electrostatic attraction between U(VI) and SiO₂/CS is strong, the adsorption manners were found to be preferable by analyzing the ΔG° of the interactions. A negative ΔH° may advise exothermic adsorption. ΔS° was negatively biased, indicating that adsorption could occur orderly at the interface between the adsorbent and the solution.

Table 5. Thermodynamic U(VI) adsorption settings at SiO₂/CS.

T, K	298	303	308	313	318	323	328
ΔG° , kJ/mol	-0.392 ± 0.05	-0.369 ± 0.08	-0.347 ± 0.09	-0.325 ± 0.06	-0.302 ± 0.05	-0.279 ± 0.07	-0.257 ± 0.06
ΔH° , kJ/mol	-1.73 ± 0.09						
ΔS° , kJ/(mol. K)	$-0.45 \times 10^{-2} \pm 0.009$						
R ²	0.9915						

3.2.6. Diverse Ions Effect

The effect of diverse ions on U(VI) sorption was studied by 50 mL of 200 mg/L U(VI), pH 3.5, and 50 mg SiO₂/CS for a 50 min time of adsorption. Different binary mixtures containing U(VI) ions and the other diverse ions were contacted together under the optimized conditions of U(VI) sorption. The diverse ions were prepared from their salts and added to the original solution. The distribution ratio (D) is calculated from the ratio of metal ions in the solid phase (C_S) to their concentration in the aqueous phase (C_A).

$$D = C_S/C_A \quad (10)$$

The separation factor (β) indicates the selectivity of the SiO₂/CS towards U(VI) in the presence of diverse ions.

$$\beta = D_U/D_M \quad (11)$$

where D_U and D_M are the distribution ratio of uranium and diverse metals, respectively. Furthermore, the tolerance limit is determined and defined as the concentration of diverse ions (mg/L) that cause an error in U(VI) recovery not exceeding $\pm 2\%$. The possible interference of the associated elements leads to adverse effects on the U(VI) sorption if the diverse metal ions are reacted or sorbed on the SiO₂/CS active sites. These ions also compete with uranium sorption. From the obtained results in Table 6, it is found that the ions such as Na⁺, K⁺, Ca²⁺, Mg²⁺, Al³⁺, Si⁴⁺, P⁵⁺, and Ba²⁺ do not interfere with 200 mg/L U(VI) to the limit of 2000 mg/L whereas these diverse ions can be tolerated to a greater extent. At the same time, ions such as Ti⁴⁺, Cr³⁺, Ni²⁺, Cu²⁺, Zn²⁺, Mn²⁺, Zr⁴⁺, Pb²⁺, V⁵⁺, and Fe³⁺ interfere with 200 mg/L U(VI) till a certain limit, whereas these ions do interfere with U(VI) sorption. The results show that SiO₂/CS is selective in extracting U(VI) from the diverse ions, whereas the separation factor values of SiO₂/CS are higher.

3.3. Adsorption Mechanism

Prior to and following U(VI) adsorption, XRD, SEM, EDX, and FTIR analysis provided valuable information. Figure 1 shows the XRD patterns. The high-intensity CS peak positions and shapes overlapped with the SiO₂ peak positions. The adsorption of uranium ions resulted in the appearance of new peaks in the XRD pattern of U/SiO₂/CS. An SEM image of U/SiO₂/CS (Figure 2) reveals pores filled with U(VI) and a rough, agglomerated surface of U/SiO₂/CS. The EDX spectra corresponding to the uranium ion sorption were used to identify it (Figure 2). If you look at this graph, uranium is visible at the bottom. Pore-blocking with uranium ions reduced the SiO₂/CS surface area, pore size, and pore volume, as shown in Figure 3. U(VI) ions were firmly adsorbent on the SiO₂/CS surface. There were new features of (O=U=O) at 975 and 748 cm⁻¹ in the FTIR spectra before and after the adsorption of U(VI). In addition, U-O showed two weak peaks near 490 cm⁻¹.

U(VI) attachment may occur via the deprotonation of functional groups of adsorbents, according to the pH-dependent designation (Figure 5a). The cationic species of U(VI) were found at pH 3.5. The hydroxyl, silanol (Si-OH), NH, and NH₂ groups on SiO₂/CS surfaces reacted with uranyl ions at these active sites. Chemisorption was found to control the adsorption mechanism and better fit the second-order kinetic data to the U(VI) adsorption data. The experimental data from the isotherm investigation fit the Langmuir model

perfectly. In addition, the adsorption process was exothermic and unforced. Figure 8 depicts one possible mechanism for U(VI) adsorption on the SiO₂/CS surface.

Table 6. Diverse ions effect on U(VI) sorption efficiency using SiO₂/CS.

Diverse Ions	Tolerance Limit, W/W *	Adsorption Efficiency, %	Separation Factor, β
K ⁺	2000 ± 20.17	99 ± 1.89	1 × 10 ⁵ ± 42
Na ⁺	2000 ± 19.34	99 ± 1.93	1 × 10 ⁵ ± 71
Mg ²⁺	2000 ± 21.45	99 ± 2.01	1 × 10 ⁵ ± 64
Ca ²⁺	2000 ± 22.44	99 ± 1.99	1 × 10 ⁵ ± 55
Al ³⁺	2000 ± 18.58	99 ± 1.79	1 × 10 ⁵ ± 65
Si ⁴⁺	2000 ± 19.77	99 ± 1.94	1 × 10 ⁵ ± 64
P ⁵⁺	2000 ± 20.78	99 ± 1.97	1 × 10 ⁵ ± 63
Ba ²⁺	2000 ± 21.23	99 ± 1.89	1 × 10 ⁵ ± 63
V ⁵⁺	400 ± 12.22	99 ± 1.99	1 × 10 ⁵ ± 58
Zn ²⁺	400 ± 12.22	99 ± 1.92	1.6 × 10 ⁵ ± 59
Ni ²⁺	400 ± 11.45	98 ± 1.88	1.6 × 10 ⁴ ± 47
Mn ²⁺	500 ± 10.76	99 ± 1.91	2.5 × 10 ⁴ ± 45
Cr ³⁺	400 ± 9.79	98 ± 1.89	1.6 × 10 ⁴ ± 51
Fe ³⁺	500 ± 11.23	98 ± 1.98	5 × 10 ³ ± 52
Pb ²⁺	300 ± 8.85	98 ± 1.96	1.4 × 10 ⁴ ± 61
Zr ⁴⁺	300 ± 8.81	98 ± 1.95	8.9 × 10 ³ ± 71
Ti ⁴⁺	500 ± 10.21	99 ± 1.92	2.5 × 10 ⁴ ± 59
Cu ²⁺	350 ± 8.89	99 ± 1.97	1.6 × 10 ⁴ ± 56

* Weight ratio of the individual interfering ion to that of U(VI).

3.4. U(VI) Desorption

Uranium desorption from the uranium-loaded SiO₂/CS was performed. The desorption manner is genuinely used to reuse and regenerate the adsorbent. In addition, it is a significant aspect of decreasing the adsorbent purification cost. Many aspects affect the desorption efficiency via batch methods, such as eluting concentration, S:L phase ratio, along with desorbing time [63–65].

3.4.1. Eluting Type

Applying different eluting types, such as HNO₃, HCl, H₂SO₄, NaCl, Na₂CO₃, and (NH₄)₂CO₃, affected the elution of U(VI) ions from the uranium-loaded-SiO₂/CS. Despite this, the additional desorption parameters remained constant over 60 min at room temperature and an elution concentration of 1.0 M at an S:L ratio of 1:30 (30 mL eluent to 1.0 g U/SiO₂/CS). Figure 9a illustrates that the U(VI) desorption via 1.0 M H₂SO₄ attained the maximum desorption at 82.0%. Consequently, it was settled that sulfuric acid was suitable for desorption.

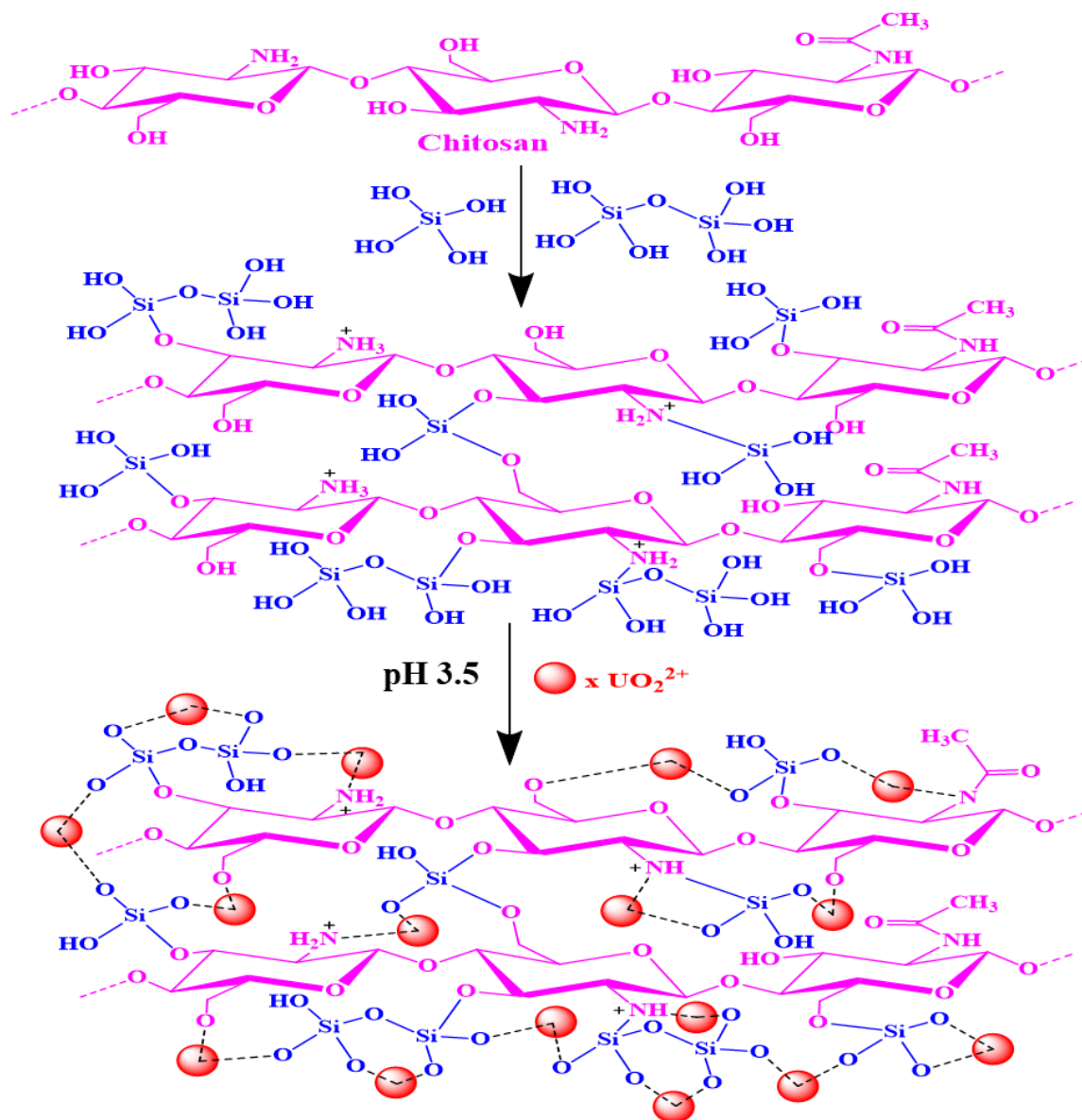


Figure 8. The graphical chart for the adsorption SiO_2/CS and U(VI) ions.

3.4.2. H_2SO_4 Concentration

The eluting concentration plays a substantial role in metal ion desorption from the loaded sorbent. Using an H_2SO_4 concentration ranging from 0.2 to 1.2 M, the U(VI) desorption from $\text{U/SiO}_2/\text{CS}$ was performed. Still, the related parameters remained constant at 1.0 g, S:L phase ratio of 1:30, and 60 min of contact time at room temperature. Figure 9b shows that by increasing the H_2SO_4 concentration from 0.2 to 0.8 M, the desorption rate increased to 82.0%. Accordingly, 0.8 M H_2SO_4 was chosen for the subsequent desorption procedure.

3.4.3. S:L Phase Ratio

Identifying the most acceptable minimum eluent volume to elute the U(VI) ions from $\text{U/SiO}_2/\text{CS}$ is significant. To examine the minimum eluting volume for the U(VI) desorption from $\text{U/SiO}_2/\text{CS}$, various volumes of 0.8 M sulfuric acid were used in the range from 10 to 70 mL, which was added to 1.0 g $\text{U/SiO}_2/\text{CS}$ for 60 min desorbing time (Figure 9c). As the S:L phase ratio decreased to 1:50, the data showed that the desorption of

uranium ions increased; after this, the U(VI) desorption remained nearly constant at 92.0%. As a result, the following experiments used an S:L ratio U/SiO₂/CS of 1:50.

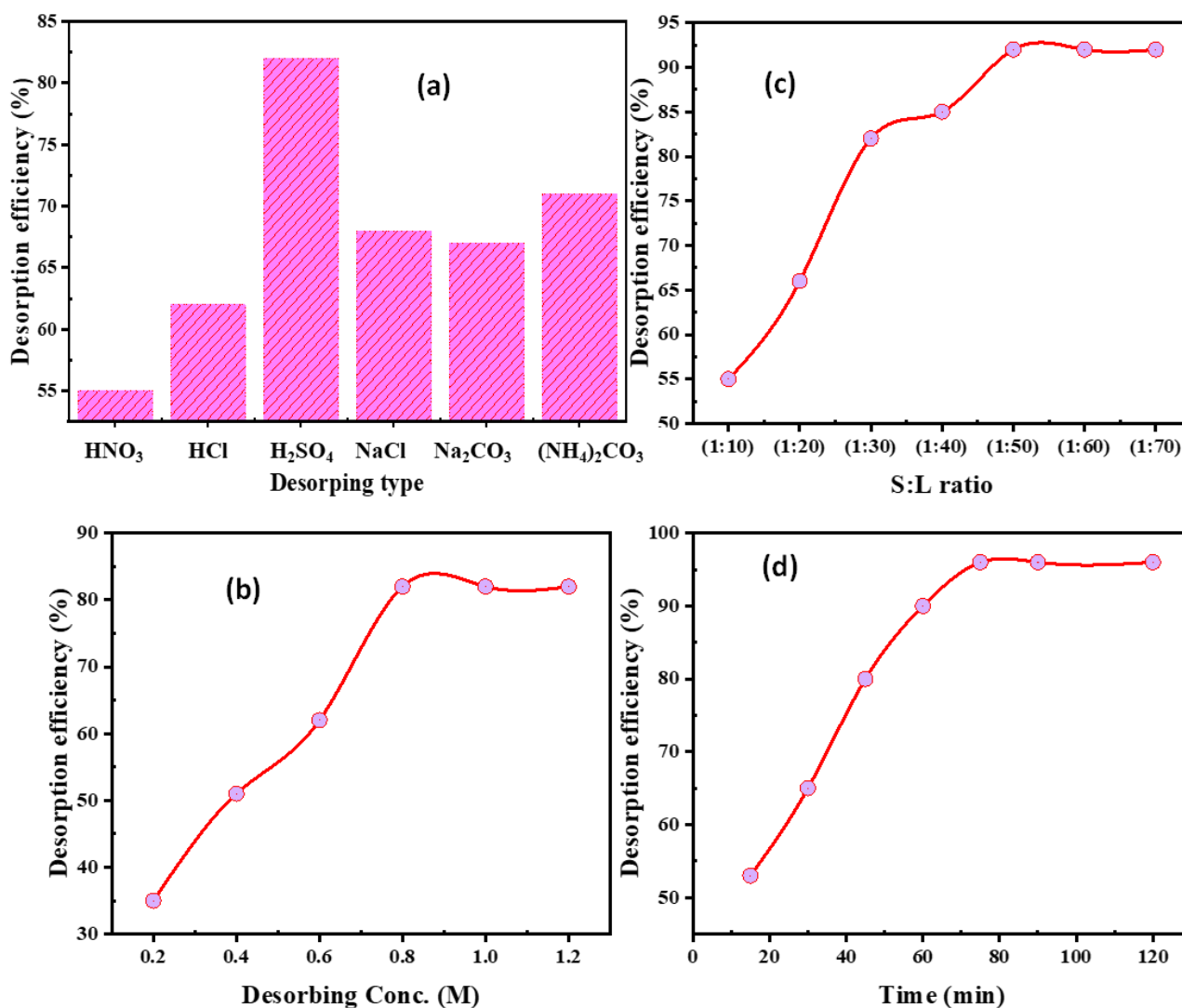


Figure 9. (a) Eluting agent, (b) H₂SO₄ desorbing concentration, (c) S:L phase ratio, and (d) desorbing time influence upon U(VI) desorption for the U/SiO₂/CS.

3.4.4. Desorbing Time

At room temperature, 50 mL of 0.8 M H₂SO₄ was used to stir 1 g U/SiO₂/CS for contact time ranging from 10 to 120 min. Figure 9d shows that the best time for maximum desorption (96.0%) was 75 min of contact time and remained constant, indicating that the system had reached equilibrium. As a result, 75 min was the optimal desorption time.

3.5. Regeneration of the SiO₂/CS

The reusable U/SiO₂/CS has undergone regeneration multiple times. Then, 0.8 M of H₂SO₄ and a 1:50 S:L ratio were used to regenerate the U/SiO₂/CS for 75 min at ambient temperature. The sorption–desorption developments were recurrent many times till desorption reduced from 96.0 to 81.0% after seven consecutive series. It designated the good adsorption constancy of the SiO₂/CS for uranium recovery.

4. Conclusions

A simple hydrothermal process can be used to make nano silica/chitosan (SiO₂/CS). The analyzing methods used to characterize the SiO₂/CS prepared include those listed above and EDX analysis, BET, and FTIR. At pH 3.5 and 200 mg/L, metal ions, 50 min of sorbing time, and 50 mm of SiO₂/CS were used to remove U (VI). The data showed that a sorption uptake of 165 mg/g was optimal. The investigation results revealed that the SiO₂/CS imitated U(VI) adsorption followed a monolayer chemical sorption progression and was consistent with second-order kinetic and Langmuir models. Adsorption on SiO₂/CS was an exothermic and spontaneous development. To reuse and recycle the SiO₂/CS, a desorption process using 0.8 M H₂SO₄ and a 1:50 S:L phase ratio was carried out for 75 min. It took seven series for the desorption to drop from 96.0 to 81.0 percent, but it eventually stabilized. Using the SiO₂/CS adsorbent developed in this study, U(VI) adsorption was found to be very effective.

Author Contributions: Conceptualization, A.K.S.; methodology, S.M.A.D.; software, M.F.C.; validation, M.Y.H.; formal analysis, K.A.A.E.-R.; investigation, E.M.A.; resources, M.F.C.; data curation, M.M.A.A.; writing—original draft preparation, M.F.C.; writing—review and editing, A.K.S.; visualization, A.K.S.; supervision, M.F.C.; project administration, E.A.E.; funding acquisition, M.S.A. All authors have read and agreed to the published version of the manuscript.

Funding: The Ministry of Education in KSA, grant number IFP-KKU-2020/14.

Data Availability Statement: Not applicable.

Acknowledgments: The authors extend their appreciation to the Ministry of Education in KSA for funding this research through project number IFP-KKU-2020/14.

Conflicts of Interest: The authors declare no conflict of interest.

References

1. Yusuf, A.; Sodiq, A.; Giwa, A.; Eke, J.; Pikuda, O.; De Luca, G.; Di Salvo, J.L.; Chakraborty, S. A review of emerging trends in membrane science and technology for sustainable water treatment. *J. Clean. Prod.* **2020**, *266*, 121867. [[CrossRef](#)]
2. Das, T.K.; Poater, A. Review on the Use of Heavy Metal Deposits from Water Treatment Waste towards Catalytic Chemical Syntheses. *Int. J. Mol. Sci.* **2021**, *22*, 13383. [[CrossRef](#)]
3. Chen, C.; Wang, J. Uranium removal by novel graphene oxide-immobilized *Saccharomyces cerevisiae* gel beads. *J. Environ. Radioact.* **2016**, *162*, 134–145. [[CrossRef](#)]
4. Ye, Y.; Jin, J.; Chen, F.; Dionysiou, D.D.; Feng, Y.; Liang, B.; Cheng, H.-Y.; Qin, Z.; Tang, X.; Li, H.; et al. Removal and recovery of aqueous U(VI) by heterogeneous photocatalysis: Progress and challenges. *Chem. Eng. J.* **2022**, *450*, 138317. [[CrossRef](#)]
5. Du, J.; Waite, T.D.; Biesheuvel, P.M.; Tang, W. Recent advances and prospects in electrochemical coupling technologies for metal recovery from water. *J. Hazard. Mater.* **2023**, *442*, 130023. [[CrossRef](#)]
6. Gurreri, L.; Tamburini, A.; Cipollina, A.; Micale, G. Electrodialysis Applications in Wastewater Treatment for Environmental Protection and Resources Recovery: A Systematic Review on Progress and Perspectives. *Membranes* **2020**, *10*, 146. [[CrossRef](#)]
7. Sakr, A.K.; Al-Hamarneh, I.F.; Goma, H.; Abdel Aal, M.M.; Hanfi, M.Y.; Sayyed, M.I.; Khandaler, M.U.; Cheira, M.F. Removal of uranium from nuclear effluent using regenerated bleaching earth steeped in β -naphthol. *Radiat. Phys. Chem.* **2022**, *200*, 110204. [[CrossRef](#)]
8. Kegl, T.; Kořak, A.; Lobnik, A.; Novak, Z.; Kralj, A.K.; Ban, I. Adsorption of rare earth metals from wastewater by nanomaterials: A review. *J. Hazard. Mater.* **2020**, *386*, 121632. [[CrossRef](#)]
9. Xu, C.; Wang, J.; Yang, T.; Chen, X.; Liu, X.; Ding, X. Adsorption of uranium by amidoximated chitosan-grafted polyacrylonitrile, using response surface methodology. *Carbohydr. Polym.* **2015**, *121*, 79–85. [[CrossRef](#)]
10. Pastoor, K.J.; Miskowicz, A.J.; Niedziela, J.L.; Christian, J.H.; Foley, B.J.; Isbill, S.B.; Shields, A.E.; Manjón-Sanz, A.M.; Nykwest, E.C.; Spano, T.L.; et al. Structural Characterization of Uranium Tetrafluoride Hydrate (UF₄·2.5H₂O). *J. Phys. Chem. C* **2022**, *126*, 13256–13267. [[CrossRef](#)]
11. Sang, K.; Mei, D.; Wang, Y.; Liu, L.; Li, H.; Yang, G.; Ma, F.; Zhang, C.; Dong, H. Amidoxime-functionalized zeolitic imidazolate frameworks with antimicrobial property for the removal of U (VI) from wastewater. *J. Environ. Chem. Eng.* **2022**, *10*, 108344. [[CrossRef](#)]
12. Xiong, T.; Jia, L.; Li, Q.; Zhang, Y.; Zhu, W. Efficient removal of uranium by hydroxyapatite modified kaolin aerogel. *Sep. Purif. Technol.* **2022**, *299*, 121776. [[CrossRef](#)]
13. Wang, G.; Liu, J.; Wang, X.; Xie, Z.; Deng, N. Adsorption of uranium (VI) from aqueous solution onto cross-linked chitosan. *J. Hazard. Mater.* **2009**, *168*, 1053–1058. [[CrossRef](#)]

14. Ao, X.; Zhou, L.; Yu, H.; Ouyang, J.; Liu, Z.; Liu, Y.; Adesina, A.A. Polyethyleneimine incorporated chitosan/ α -MnO₂ nanorod honeycomb-like composite foams with remarkable elasticity and ultralight property for the effective removal of U(VI) from aqueous solution. *Int. J. Biol. Macromol.* **2022**, *218*, 190–201. [[CrossRef](#)]
15. Anpo, M.; Costentin, G.; Giamello, E.; Lauron-Pernot, H.; Sojka, Z. Characterisation and reactivity of oxygen species at the surface of metal oxides. *J. Catal.* **2021**, *393*, 259–280. [[CrossRef](#)]
16. Vassileva, E.; Proinova, I.; Hadjiivanov, K. Solid-phase extraction of heavy metal ions on a high surface area titanium dioxide (anatase). *Analyst* **1996**, *121*, 607–612. [[CrossRef](#)]
17. Fan, F.-L.; Qin, Z.; Bai, J.; Rong, W.-D.; Fan, F.-Y.; Tian, W.; Wu, X.-L.; Wang, Y.; Zhao, L. Rapid removal of uranium from aqueous solutions using magnetic Fe₃O₄@SiO₂ composite particles. *J. Environ. Radioact.* **2012**, *106*, 40–46. [[CrossRef](#)]
18. Tashkhourian, J.; Moradi Abdolousofi, L.; Pakniat, M.; Montazerzohori, M. Sodium dodecyl sulfate coated alumina modified with a new Schiff's base as a uranyl ion selective adsorbent. *J. Hazard. Mater.* **2011**, *187*, 75–81. [[CrossRef](#)]
19. Sylwester, E.R.; Hudson, E.A.; Allen, P.G. The structure of uranium (VI) sorption complexes on silica, alumina, and montmorillonite. *Geochim. Cosmochim. Acta* **2000**, *64*, 2431–2438. [[CrossRef](#)]
20. Wang, J.; Zhuang, S. Extraction and adsorption of U(VI) from aqueous solution using affinity ligand-based technologies: An overview. *Rev. Environ. Sci. Bio/Technol.* **2019**, *18*, 437–452. [[CrossRef](#)]
21. Hassanin, M.A.; El-Gendy, H.S.; Cheira, M.F.; Atia, B.M. Uranium ions extraction from the waste solution by thiosemicarbazide anchored cellulose acetate. *Int. J. Environ. Anal. Chem.* **2021**, *101*, 351–369. [[CrossRef](#)]
22. Gunathilake, C.; Górká, J.; Dai, S.; Jaroniec, M. Amidoxime-modified mesoporous silica for uranium adsorption under seawater conditions. *J. Mater. Chem. A* **2015**, *3*, 11650–11659. [[CrossRef](#)]
23. Amesh, P.; Venkatesan, K.A.; Suneesh, A.S.; Gupta, D.K.; Ravindran, T.R. Adsorption of uranium by diethylenetriamine functionalized magnetic mesoporous silica. *Environ. Nanotechnol. Monit. Manag.* **2021**, *16*, 100583. [[CrossRef](#)]
24. Giannakoudakis, D.A.; Anastopoulos, I.; Barczak, M.; Antoniou, E.; Terpiłowski, K.; Mohammadi, E.; Shams, M.; Coy, E.; Bakandritsos, A.; Katsoyiannis, I.A.; et al. Enhanced uranium removal from acidic wastewater by phosphonate-functionalized ordered mesoporous silica: Surface chemistry matters the most. *J. Hazard. Mater.* **2021**, *413*, 125279. [[CrossRef](#)]
25. Hamza, M.F.; Gamal, A.; Hussein, G.; Nagar, M.S.; Abdel-Rahman, A.A.H.; Wei, Y.; Guibal, E. Uranium(VI) and zirconium(IV) sorption on magnetic chitosan derivatives—Effect of different functional groups on separation properties. *J. Chem. Technol. Biotechnol.* **2019**, *94*, 3866–3882. [[CrossRef](#)]
26. Cheira, M.F. Performance of poly sulfonamide/nano-silica composite for adsorption of thorium ions from sulfate solution. *SN Appl. Sci.* **2020**, *2*, 398. [[CrossRef](#)]
27. Liu, C.; Lu, J.; Tan, Y.; Chen, B.; Yang, P. Removal of U(VI) from wastewater by sulfhydryl-functionalized biomass carbon supported nano-zero-valent iron through synergistic effect of adsorption and reduction. *Mater. Sci. Eng. B* **2022**, *284*, 115891. [[CrossRef](#)]
28. Huynh, J.; Palacio, R.; Safizadeh, F.; Lefèvre, G.; Descostes, M.; Eloy, L.; Guignard, N.; Rousseau, J.; Royer, S.; Tertre, E.; et al. Adsorption of Uranium over NH₂-Functionalized Ordered Silica in Aqueous Solutions. *ACS Appl. Mater. Interfaces* **2017**, *9*, 15672–15684. [[CrossRef](#)] [[PubMed](#)]
29. Jamali, M.R.; Assadi, Y.; Shemirani, F.; Hosseini, M.R.M.; Kozani, R.R.; Masteri-Farahani, M.; Salavati-Niasari, M. Synthesis of salicylaldehyde-modified mesoporous silica and its application as a new sorbent for separation, preconcentration and determination of uranium by inductively coupled plasma atomic emission spectrometry. *Anal. Chim. Acta* **2006**, *579*, 68–73. [[CrossRef](#)] [[PubMed](#)]
30. de Queiroz Antonino, R.; Lia Fook, B.R.P.; de Oliveira Lima, V.A.; de Farias Rached, R.; Lima, E.P.N.; da Silva Lima, R.J.; Peniche Covas, C.A.; Lia Fook, M.V. Preparation and Characterization of Chitosan Obtained from Shells of Shrimp (*Litopenaeus vannamei* Boone). *Mar. Drugs* **2017**, *15*, 141. [[CrossRef](#)]
31. Mohammed, M.H.; Williams, P.A.; Tverezovskaya, O. Extraction of chitin from prawn shells and conversion to low molecular mass chitosan. *Food Hydrocoll.* **2013**, *31*, 166–171. [[CrossRef](#)]
32. Sharma, M.; Laddha, H.; Yadav, P.; Jain, Y.; Sachdev, K.; Janu, V.C.; Gupta, R. Selective removal of uranium from an aqueous solution of mixed radionuclides of uranium, cesium, and strontium via a viable recyclable GO@chitosan based magnetic nanocomposite. *Mater. Today Commun.* **2022**, *32*, 104020. [[CrossRef](#)]
33. Mohan, K.; Ganesan, A.R.; Ezhilarasi, P.N.; Kondamareddy, K.K.; Rajan, D.K.; Sathishkumar, P.; Rajarajeswaran, J.; Conterno, L. Green and eco-friendly approaches for the extraction of chitin and chitosan: A review. *Carbohydr. Polym.* **2022**, *287*, 119349. [[CrossRef](#)] [[PubMed](#)]
34. Hassanin, M.A.; Negm, S.H.; Youssef, M.A.; Sakr, A.K.; Mira, H.I.; Mohammaden, T.F.; Al-Otaibi, J.S.; Hanfi, M.Y.; Sayyed, M.I.; Cheira, M.F. Sustainable Remedy Waste to Generate SiO₂ Functionalized on Graphene Oxide for Removal of U(VI) Ions. *Sustainability* **2022**, *14*, 2699. [[CrossRef](#)]
35. Bao, M.; Zhu, G.; Wang, L.; Wang, M.; Gao, C. Preparation of monodispersed spherical mesoporous nanosilica–polyamide thin film composite reverse osmosis membranes via interfacial polymerization. *Desalination* **2013**, *309*, 261–266. [[CrossRef](#)]
36. Budnyak, T.M.; Pylypchuk, I.V.; Tertykh, V.A.; Yanovska, E.S.; Kolodynska, D. Synthesis and adsorption properties of chitosan-silica nanocomposite prepared by sol-gel method. *Nanoscale Res. Lett.* **2015**, *10*, 87. [[CrossRef](#)]
37. Mohammed, M.I.; Ismael, M.K.; Gönen, M. Synthesis of Chitosan-Silica Nanocomposite for Removal of Methyl Orange from Water: Composite Characterization and Adsorption Performance. *IOP Conf. Ser. Mater. Sci. Eng.* **2020**, *745*, 012084. [[CrossRef](#)]

38. Abou Rida, M.; Harb, F. Synthesis and characterization of amorphous silica nanoparticles from aqueous silicates using cationic surfactants. *J. Met. Mater. Miner.* **2014**, *24*, 37–42.
39. Guo, Q.; Yang, G.; Huang, D.; Cao, W.; Ge, L.; Li, L. Synthesis and characterization of spherical silica nanoparticles by modified Stöber process assisted by slow-hydrolysis catalyst. *Colloid Polym. Sci.* **2018**, *296*, 379–384. [[CrossRef](#)]
40. Lu, P.; Hsieh, Y.-L. Highly pure amorphous silica nano-disks from rice straw. *Powder Technol.* **2012**, *225*, 149–155. [[CrossRef](#)]
41. Liu, L.; Yang, W.; Gu, D.; Zhao, X.; Pan, Q. In situ Preparation of Chitosan/ZIF-8 Composite Beads for Highly Efficient Removal of U(VI). *Front. Chem.* **2019**, *7*, 607. [[CrossRef](#)] [[PubMed](#)]
42. Zhang, L.; Zeng, Y.; Cheng, Z. Removal of heavy metal ions using chitosan and modified chitosan: A review. *J. Mol. Liq.* **2016**, *214*, 175–191. [[CrossRef](#)]
43. Monier, M.; Elsayed, N.H. Selective extraction of uranyl ions using ion-imprinted chelating microspheres. *J. Colloid Interface Sci.* **2014**, *423*, 113–122. [[CrossRef](#)] [[PubMed](#)]
44. Sun, Z.; Chen, D.; Chen, B.; Kong, L.; Su, M. Enhanced uranium(VI) adsorption by chitosan modified phosphate rock. *Colloids Surf. A Physicochem. Eng. Asp.* **2018**, *547*, 141–147. [[CrossRef](#)]
45. Sureshkumar, M.K.; Das, D.; Mallia, M.B.; Gupta, P.C. Adsorption of uranium from aqueous solution using chitosan-tripolyphosphate (CTPP) beads. *J. Hazard. Mater.* **2010**, *184*, 65–72. [[CrossRef](#)] [[PubMed](#)]
46. Zidan, I.H.; Cheira, M.F.; Bakry, A.R.; Atia, B.M. Potentiality of uranium recovery from G.Gattar leach liquor using Duolite ES-467 chelating resin: Kinetic, thermodynamic and isotherm features. *Int. J. Environ. Anal. Chem.* **2022**, *102*, 2102–2124. [[CrossRef](#)]
47. Kausar, A.; Naeem, K.; Hussain, T.; Nazli, Z.-i.-H.; Bhatti, H.N.; Jubeen, F.; Nazir, A.; Iqbal, M. Preparation and characterization of chitosan/clay composite for direct Rose FRN dye removal from aqueous media: Comparison of linear and non-linear regression methods. *J. Mater. Res. Technol.* **2019**, *8*, 1161–1174. [[CrossRef](#)]
48. Sakr, A.K.; Cheira, M.F.; Hassanin, M.A.; Mira, H.I.; Mohamed, S.A.; Khandaker, M.U.; Osman, H.; Eed, E.M.; Sayyed, M.I.; Hanfi, M.Y. Adsorption of Yttrium Ions on 3-Amino-5-Hydroxypyrazole Impregnated Bleaching Clay, a Novel Sorbent Material. *Appl. Sci.* **2021**, *11*, 10320. [[CrossRef](#)]
49. Ho, Y.S.; McKay, G. Pseudo-second order model for sorption processes. *Process Biochem.* **1999**, *34*, 451–465. [[CrossRef](#)]
50. Imam, E.A.; El-Tantawy El-Sayed, I.; Mahfouz, M.G.; Tolba, A.A.; Akashi, T.; Galhoum, A.A.; Guibal, E. Synthesis of α -aminophosphonate functionalized chitosan sorbents: Effect of methyl vs phenyl group on uranium sorption. *Chem. Eng. J.* **2018**, *352*, 1022–1034. [[CrossRef](#)]
51. Cheira, M.F.; Mira, H.I.; Sakr, A.K.; Mohamed, S.A. Adsorption of U(VI) from acid solution on a low-cost sorbent: Equilibrium, kinetic, and thermodynamic assessments. *Nucl. Sci. Tech.* **2019**, *30*, 156. [[CrossRef](#)]
52. Ilaiyaraja, P.; Singha Deb, A.K.; Sivasubramanian, K.; Ponraju, D.; Venkatraman, B. Adsorption of uranium from aqueous solution by PAMAM dendron functionalized styrene divinylbenzene. *J. Hazard. Mater.* **2013**, *250*, 155–166. [[CrossRef](#)] [[PubMed](#)]
53. Weshahy, A.R.; Sakr, A.K.; Gouda, A.A.; Atia, B.M.; Somaily, H.H.; Hanfi, M.Y.; Sayyed, M.I.; El Sheikh, R.; El-Sheikh, E.M.; Radwan, H.A.; et al. Selective Recovery of Cadmium, Cobalt, and Nickel from Spent Ni–Cd Batteries Using Adogen®464 and Mesoporous Silica Derivatives. *J. Mol. Sci.* **2022**, *23*, 8677. [[CrossRef](#)] [[PubMed](#)]
54. Jung, Y.; Kim, S.; Park, S.-J.; Kim, J.M. Application of polymer-modified nanoporous silica to adsorbents of uranyl ions. *Colloids Surf. A Physicochem. Eng. Asp.* **2008**, *313*, 162–166. [[CrossRef](#)]
55. Donia, A.M.; Atia, A.A.; Daher, A.M.; Desouky, O.A.; Elshehy, E.A. Selective separation of U(VI) from its solutions using amine modified silica gel produced from leached zircon. *Int. J. Miner. Process.* **2011**, *101*, 81–88. [[CrossRef](#)]
56. Mishima, K.; Du, X.; Miyamoto, N.; Kano, N.; Imaizumi, H. Experimental and Theoretical Studies on the Adsorption Mechanisms of Uranium (VI) Ions on Chitosan. *J. Funct. Biomater.* **2018**, *9*, 49. [[CrossRef](#)]
57. Negm, S.H.; Abd El-Magied, M.O.; El Maadawy, W.M.; Abdel Aal, M.M.; Abd El Dayem, S.M.; Taher, M.A.; Abd El-Rahem, K.A.; Rashed, M.N.; Cheira, M.F. Appreciatively Efficient Sorption Achievement to U(VI) from the El Sela Area by ZrO₂/Chitosan. *Separations* **2022**, *9*, 311. [[CrossRef](#)]
58. Szlachta, M.; Neitola, R.; Peräniemi, S.; Vepsäläinen, J. Effective separation of uranium from mine process effluents using chitosan as a recyclable natural adsorbent. *Sep. Purif. Technol.* **2020**, *253*, 117493. [[CrossRef](#)]
59. Zhang, Q.; Zhang, S.; Zhao, J.; Wei, P.; Wang, C.; Liu, P.; Zhao, X.; Zeng, K.; Wu, F.; Liu, Z. Unexpected ultrafast and highly efficient removal of uranium from aqueous solutions by a phosphonic acid and amine functionalized polymer adsorbent. *New J. Chem.* **2021**, *45*, 10777–10787. [[CrossRef](#)]
60. Zhang, Q.; Wang, Y.; Wang, Z.; Zhang, Z.; Wang, X.; Yang, Z. Active biochar support nano zero-valent iron for efficient removal of U(VI) from sewage water. *J. Alloys Compd.* **2021**, *852*, 156993. [[CrossRef](#)]
61. Abdel Geleel, M.; Atwa, S.T.; Sakr, A.K. Removal of Cr (III) from aqueous waste using Spent Activated Clay. *J. Am. Sci.* **2013**, *9*, 256–262.
62. Mahmoud, N.S.; Atwa, S.T.; Sakr, A.K.; Abdel Geleel, M. Kinetic and thermodynamic study of the adsorption of Ni (II) using Spent Activated clay Mineral. *N. Y. Sci. J.* **2012**, *5*, 62–68. [[CrossRef](#)]
63. Atia, B.M.; Sakr, A.K.; Gado, M.A.; El-Gendy, H.S.; Abdelazeem, N.M.; El-Sheikh, E.M.; Hanfi, M.Y.; Sayyed, M.I.; Al-Otaibi, J.S.; Cheira, M.F. Synthesis of a New Chelating Iminophosphorane Derivative (Phosphazene) for U(VI) Recovery. *Polymers* **2022**, *14*, 1687. [[CrossRef](#)] [[PubMed](#)]

64. Allam, E.M.; Lashen, T.A.; Abou El-Enein, S.A.; Hassanin, M.A.; Sakr, A.K.; Hanfi, M.Y.; Sayyed, M.I.; Al-Otaibi, J.S.; Cheira, M.F. Cetylpyridinium Bromide/Polyvinyl Chloride for Substantially Efficient Capture of Rare Earth Elements from Chloride Solution. *Polymers* **2022**, *14*, 954. [[CrossRef](#)] [[PubMed](#)]
65. Allam, E.M.; Lashen, T.A.; Abou El-Enein, S.A.; Hassanin, M.A.; Sakr, A.K.; Cheira, M.F.; Almuqrin, A.; Hanfi, M.Y.; Sayyed, M.I. Rare Earth Group Separation after Extraction Using Sodium Diethyldithiocarbamate/Polyvinyl Chloride from Lamprophyre Dykes Leachate. *Materials* **2022**, *15*, 1211. [[CrossRef](#)]